Macromolecular Journals

Macromolecular Chemistry and Physics

High-Performance Polybenzoxazine Nanocomposites Containing Multifunctional POSS Cores Presenting Vinyl-Terminated Benzoxazine Groups

Kai-Wei Huang, Shiao-Wei Kuo*

We have prepared a new class of polybenzoxazine/POSS nanocomposites through the reactions of a multifunctional vinyl-terminated VBa-POSS with a VBa monomer at various compositional ratios. The incorporation of the silsesquioxane core units into the polybenzoxazine matrix significantly hindered the mobility of the polymer chains and enhanced the thermal stability of these hybrid materials. Increasing the POSS content in these hybrids improved their thermal and mechanical properties, relative to those of the neat polybenzoxazine, because of hydrogen bonding between the siloxane groups of the POSS core units and the OH groups of the polybenzoxazine moieties, as adjudged using FTIR spectroscopy.

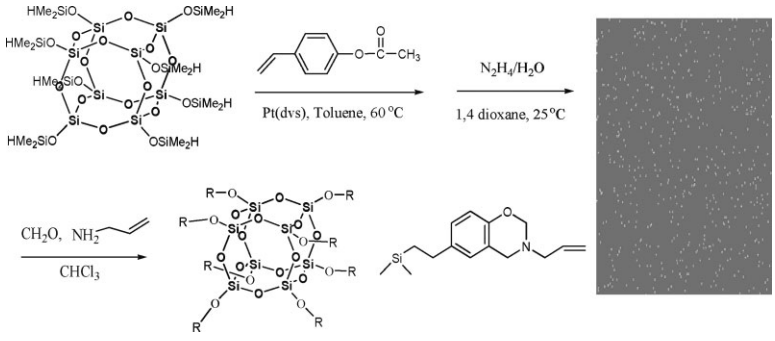

Introduction

1,3-Benzoxazines are intriguing heterocyclic (oxazine-containing) compounds that have attracted considerable attention for their use as cyclic monomers. They are synthesized through the reactions of primary amines with phenol and formaldehyde; they can be polymerized through ring-opening polymerization in the absence of a catalyst, releasing no byproducts.[1] Furthermore, polybenzoxazines have unique properties such as excellent dimensional stability, flame retardancy, stable dielectric constants, and low surface free energy not found in traditional phenolic resins.[2–7]

To improve the performance of polybenzoxazines, polymerizable alkynyl and allyl side groups have been introduced into the benzoxazine monomers.[8–16] These functionalized benzoxazines can be polymerized into products possessing three-dimensional networks that display high thermal and mechanical stability and high solvent and moisture resistances. Another approach toward improving the stability of polybenzoxazines is their blending with other polymers,[17–19] or inorganic materials. The development of polymer/inorganic nanocomposites possessing attractive properties has attracted much research interest in recent years. If the two components are miscible at the nanometer level, they usually perform better than conventional composites. Blends of polymers and montmorillonite (clay) have been studied extensively because a small amount of well-

K.-W. Huang, S.-W. Kuo
Department of Materials and Optoelectronic Science, Center for Nanoscience and Nanotechnology, National Sun Yat-Sen University, Kaohsiung 804, Taiwan
Fax: +886 7 525 4099; E-mail: kuosw@faculty.nsysu.edu.tw

DOI: 10.1002/macp.201000362

dispersed clay in a polymer matrix can improve its mechanical and thermal properties. The inorganic layered silicate structure of clay, however, does not permit its high dispersion in the organic polymer matrix; therefore, it is essential to pre-treat the clay with appropriate surfactants.[20–22] Recently, novel classes of organic/inorganic hybrid materials based on polyhedral oligomeric silsesquioxanes (POSS) have been developed.[23–34] POSS possess an inorganic Si_8O_{12} core, which can be selectively functionalized with seven inert organic hydrocarbon groups and one reactive functional group, or with eight reactive functional groups that may undergo polymerization or cross-linking.[35–44] When these inorganic POSS particles are distributed evenly within the organic matrix on the nanometer scale (1–100 nm), they usually improve the thermal stability and mechanical strength dramatically.[45–47] Unlike clays or conventional fillers, POSS derivatives are monodisperse, with well-defined molecular weights and structures, low densities, and high-temperature stabilities; they contain no trace metals and exhibit sizable interfacial free energies for their interactions with polymer segments. Because POSS compounds can contain one or more reactive sites, they are readily incorporated into common polymers. To improve the properties of polybenzoxazine, a POSS derivative can be introduced directly into a matrix featuring polymerizable groups.[48–55]

In this study, we combined the advantages of using an allyl-functionalized benzoxazine and POSS nanocomposites to enhance the thermal and mechanical properties of the resulting polybenzoxazine matrix. Previously, Lee et al.[46] prepared a monofunctional benzoxazine-substituted POSS (BZ-POSS) through hydrosilylation of a vinyl-terminated benzoxazine (VBa) with a hydrosilane POSS derivative (H-POSS) and then its incorporation into P(B-a) and P(P-a)-type polybenzoxazine matrices through ring-opening polymerization. They also reacted mono- and multi-hydrosilane-functionalized POSS derivatives with the VBa monomer and then subjected the products to ring-opening polymerizations; they found that the glass transition temperature (T_g) increased upon increasing the POSS content. In addition, the blending of a non-reactive POSS derivative (isobutyl-POSS) with VBa resulted in polymers exhibiting lower values of T_g than that of the pure polymerized VBa (PVBa) because of poor miscibility between isobutyl-POSS and VBa. In the syntheses of all of these polybenzoxazine/POSS nanocomposites, allyl groups were absent during the ring opening polymerizations.

In this study, we synthesized a multifunctional POSS bearing eight VBa-POSS groups from the reaction of octaphenol POSS[56–59] with formaldehyde and allyl amine; we then copolymerized it with VBa benzoxazine monomers through ring opening polymerization. Because these polybenzoxazine/POSS hybrid materials incorporate large numbers of POSS units into their polybenzoxazines, they exhibit notably improved thermal and mechanical stability, as evidenced through thermogravimetric analysis (TGA) and dynamic mechanical analysis (DMA).

Experimental Part

Materials

Paraformaldehyde and allylamine were purchased from Tokyo Kasei Kogyo Co. (Japan). The platinum complex (Pt-dvs, 2 wt.-% Pt in xylene) was purchased from Aldrich (USA). Prior to use, the solution of the Pt complex was diluted 100-fold with xylene. Toluene was dried by distillation prior to use in the hydrosilylation reactions. Octakis(dimethylsiloxy)silsesquioxane ($Q_8M_8^H$), which contains eight hydrosilane groups, was purchased from Hybrid Plastics Co. (USA). The benzoxazine monomer VBa was prepared according to reported procedures.[37] Octakis[dimethyl(4-hydroxyphenethyl)-siloxy]silsesquioxane (OP-POSS) was prepared through hydrosilylation of 4-acetoxystyrene with $Q_8M_8^H$ and subsequent hydrolysis of the acetoxy units.[56–59]

Preparation of Multifunctional VBa-POSS

Vinyl-terminated benzoxazine POSS was synthesized using the procedure presented in Scheme 1. Paraformaldehyde (0.93 g) was added at room temperature to a solution of OP-POSS (2.23 g) and allylamine (0.89 g) in $CHCl_3$ in a 50-mL three-neck flask. After stirring for 30 min, the temperature was raised gradually to 90 °C and then the mixture was heated under reflux for 4 h. The product was precipitated by pouring the mixture into rapidly stirred ethyl ether (40 mL). The resultant product was collected by filtration and dried in a vacuum oven to yield VBa-POSS as a viscous yellow liquid.

Preparation of VBa-Type Polybenzoxazine and VBa-POSS Hybrids

Both the VBa monomer and VBa-POSS are soluble in tetrahydrofuran (THF) and then this solution is allowed to dry in air prior to curing. A desired amount of the VBa-type benzoxazine monomer and VBa-POSS was stirred for 2 h at room temperature and then poured onto an aluminum plate to dry for 6 h in the open air before being placed in an oven at 100 °C under vacuum for 2 h. The cast film was polymerized in a stepwise manner, at 140 and 160 °C for 3 h each and then at 200 °C for 4 h. The product was post-cured at 220 and 240 °C for 30 min each. Each cured sample was transparent and had a dark red color (thickness: ca. 0.2 mm).

Characterization

^{1}H NMR spectra were obtained using an INOVA 500 instrument. FTIR spectra of the polymer blend films were recorded using the conventional KBr disk method. The films used in this study were sufficiently thin to obey the Beer-Lambert law. Fourier-transform infrared (FTIR) spectra were recorded using a Bruker Tensor 27 FTIR spectrophotometer; 32 scans were collected at a spectral resolution 1 cm^{-1}. Because polymers containing OH groups are hygroscopic, pure N_2 gas was used to purge the spectrometer's optical box to maintain dry sample films. Generalized two-dimensional (2D)

Macromol. Chem. Phys. **2010**, *211*, 2301–2311

Macromolecular Journals

DOI: 10.1002/macp.201000362

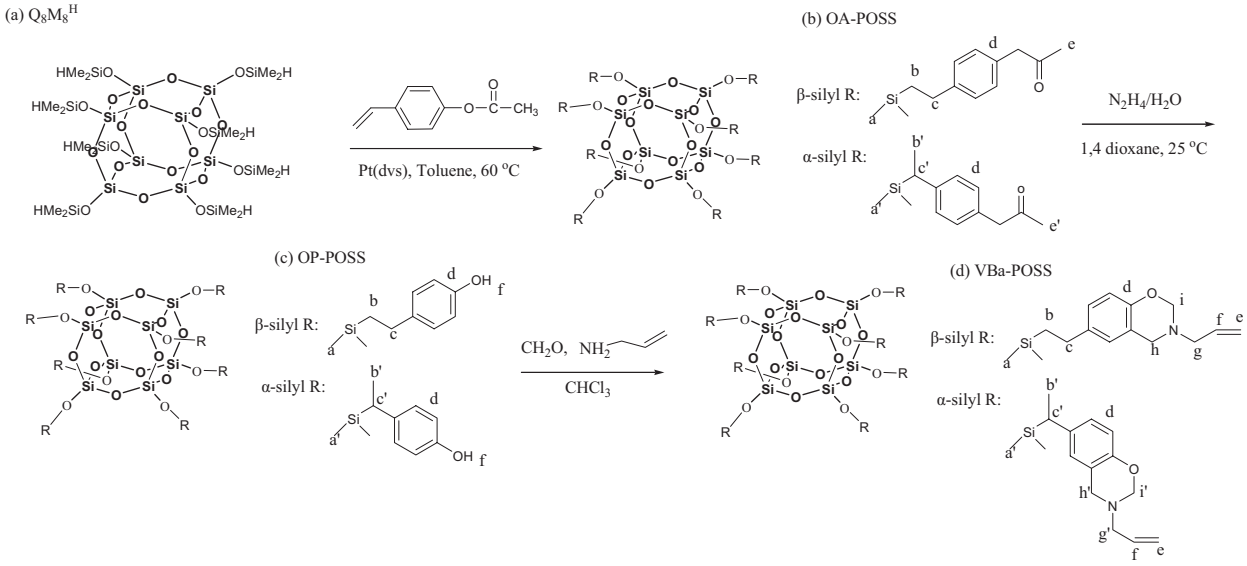

Scheme 1. Chemical structures and reaction schemes for the syntheses of (a) $Q_8M_8^H$, (b) OA-POSS, (c) OP-POSS, and (d) VBa-POSS.

correlation analysis was performed using the 2D Shige software developed by Shigeaki Morita (Kwansei-Gakuin University, Japan). In the 2D correlation maps, white-colored regions are defined as positive correlation intensities; shaded regions are defined as negative correlation intensities. The dynamic curing kinetics were studied under a N_2 atmosphere using a TA Q-20 differential scanning calorimeter. The sample (ca. 7 mg) was placed in a sealed aluminum sample pan. Dynamic curing scans were conducted from 30 to 350 °C at a heating rate of 10 °C · min^{-1}. The dynamic mechanical behavior of each cured sample was studied using a DuPont 2980 dynamic mechanical analyzer. The cured sample was polished to ca. 3.0 × 13.0 × 30.0 mm^3 and then mounted on a single cantilever clamp. The mechanical properties were measured under N_2 in step mode every 5 °C from 25 to 350 °C at a frequency (*r*) of 1 Hz. The thermal stability of each sample was characterized under a N_2 atmosphere using a TA Q-50 thermogravimetric analyzer. The cured sample (ca. 7 mg) was placed in a Pt cell and heated at a rate of 20 °C · min^{-1} from 30 to 800 °C at a N_2 flow rate of 60 mL · min^{-1}. To observe the phase structures of the polybenzoxazine/POSS nanocomposites, samples were prepared using curing reactions. The fractured surfaces were immersed in CH_2Cl_2 at room temperature for 30 min. The POSS phases were preferentially etched by the solvent; the VBa matrix phases remained unaffected. The fracture surfaces were coated with thin layers of gold (ca. 100 Å). All specimens were examined using an FEI Quanta 200 environmental scanning electron microscope operated at 20 kV.

Results and Discussion

Synthesis of VBa-POSS

Figure 1a displays the ^{1}H NMR spectra of octakis[dimethyl(4-acetoxyphenethyl)siloxy]silsesquioxane (OA-POSS). Signals for the vinyl ($\delta \approx 5.8$) and SiH protons ($\delta \approx 4.7$) are absent in this spectrum, confirming that the hydrosilylation reaction had reached completeness. The spectrum reveals that the vinyl groups of acetoxystyrene underwent hydrosilylation of the Si–H bonds of $Q_8M_8^H$ in both α and β configurations, i.e., OA-POSS features a mixture of these two orientations. From integration of the signals for the protons on the benzylic carbon atoms marked *b* (2H, β-side groups) and *b'* (1H, α-side groups), we estimated the molar ratio of β to α linkages to be 1.82:1. We used acetoxyl-hydrazinolysis (Scheme 1c) with hydrazine monohydrate to selectively deprotect the acetyl groups from OA-POSS at 25 °C for 2 h to obtain OP-POSS in high yield. The ^{1}H NMR spectrum of OP-

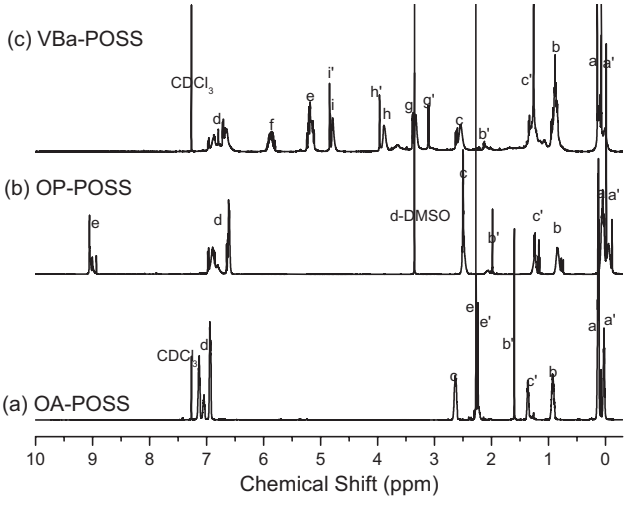

Figure 1. ^{1}H NMR spectra of (a) OA-POSS in $CDCl_3$, (b) OP-POSS in deuterated dimethyl sulfoxide (DMSO-d_6), and (c) VBa-POSS in $CDCl_3$.

POSS (Figure 1b) reveals the absence of a signal at 2.2 ppm for the acetoxy groups ($\mathbf{H}_e$); in addition, a peak ($\delta = 9.0$) corresponding to the protons of the OH groups appeared after hydrolysis. Figure 1c displays the ^{1}H NMR spectrum of VBa-POSS. The signal for the OH groups is absent; signals appear at $\delta = 3.9$ and 4.8, corresponding to the methylene bridge protons of the oxazine unit. The vinyl group appears as two signals, at $\delta = 5.21$ and 5.88, in a 2:1 ratio. The aromatic protons appear as a multiplet at $\delta = 6.77$–7.16. The signals of the protons located between the vinyl groups and the nitrogen atoms appear at $\delta = 3.37$ and 3.13, confirming that two isomers exist in VBa-POSS (α and β linkages), as indicated in Scheme 1d. Figure 2 shows the ^{29}Si NMR of $Q_8M_8^H$, OA-POSS, OP-POSS, and VBa-POSS. The peaks at –109.3, ppm are represented for the siloxane core, whose signal-to-noise ratio will dominate the spectrum. In addition, the peak at $\delta = -2.1$ are known for –O-**Si**$(CH_3)_2$H of $Q_8M_8^H$ and after hydrosilylation with 4-acetoxystyrene, it would split into two peaks at $\delta = 10.2$ and 11.9 for $-O-\mathbf{Si}(CH_3)_2-CH_2-CH_2-C_6H_4-OAc$ and $-O-\mathbf{Si}(CH_3)_2-CH(CH_3)-C_6H_4-OAc$, respectively. Clearly, the chemical shift indicates that the hydrosilylation reaction occurred to completion under the reaction conditions. After hydrazinolysis, these two peaks shift to $\delta = 10.6$ and 13.7 for $-O-\mathbf{Si}(CH_3)_2-CH_2-CH_2-C_6H_4-OH$ and $-O-\mathbf{Si}(CH_3)_2-CH(CH_3)-C_6H_4-OH$, respectively. These two peaks did not change of VBa-POSS when compared with OP-POSS.

Figure 3 presents the FTIR spectra of $Q_8M_8^H$, OA-POSS, OP-POSS, and VBa-POSS. The strong absorption signal at ca. 1 100 cm^{-1} for each compound represents the vibrations of the siloxane Si–O–Si groups; this signal is a general feature of all POSS derivatives. The characteristic stretching vibrations of the Si–H groups of $Q_8M_8^H$ appear at 2 200 cm^{-1} (Figure 3a). For OA-POSS, this peak was absent, indicating that the hydrosilylation had reached completion. Furthermore, a peak was present for the C=O groups from the acetoxystyrene units (1 765 cm^{-1}), providing evidence for the successful attachment of the acetoxystyrene units to the POSS core. The spectrum of OP-POSS after hydrolysis (Figure 3c) lacks the C=O stretching vibration; a broad peak at 3 350 cm^{-1} indicates the presence of OH groups. The FTIR spectrum of VBa-POSS (Figure 3d) lacks a signal for the OH groups; signals for carbon–carbon stretching vibrations of 1,2,4-substituted benzene rings and for asymmetric C–O–C stretchings appear at 1 490 and 1 230 cm^{-1}, respectively. In addition, the characteristic absorption bands of the allyl group appear at 3 075 (stretching of =C–H bonds) and 1 644 (stretching of C=C bonds) cm^{-1}, with out-of-plane bending vibrations of the olefinic CH bonds appearing at 860–864 and 991–997 cm^{-1}.[15] Thus, the ^{1}H, ^{29}Si NMR and FTIR spectra are indicative of the successful preparation of VBa-POSS.

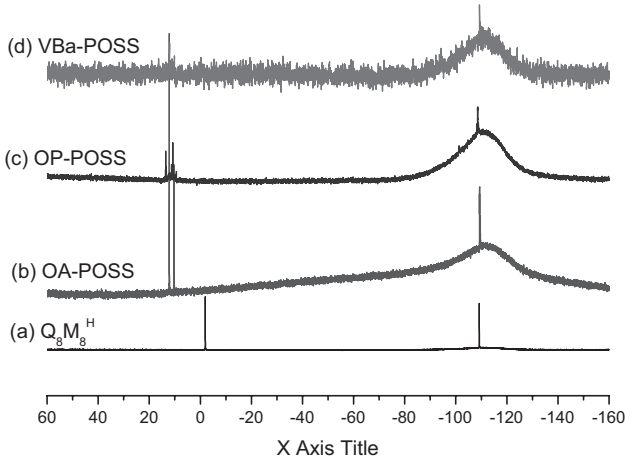

Figure 2. ^{29}Si NMR spectra of (a) $Q_8M_8^H$ in $CDCl_3$, (b) OA-POSS in $CDCl_3$, (c) OP-POSS in DMSO-d_6, and (d) VBa-POSS in $CDCl_3$.

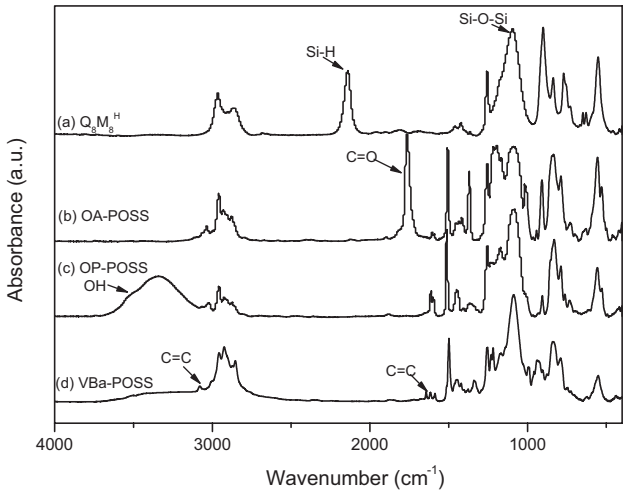

Figure 3. FTIR spectra of (a) $Q_8M_8^H$, (b) OA-POSS, (c) OP-POSS, and (d) VBa-POSS.

Thermal Polymerization of VBa-POSS

We used DSC analysis to investigate the curing behavior of pure VBa-POSS. For uncured VBa-POSS (Figure 4a), we observed two exotherms, similar to those observed for pure VBa. The onset temperature of the first exotherm was ca. 180 °C with an exotherm peak at 234 °C; the apparent onset of the second exotherm was at 245 °C with an exotherm maximum at 270 °C, when heating at a rate of 10 °C · min^{-1}.[10] The two exotherms are responsible for both allyl and benzoxazine polymerization.[8,60,61] The total exotherm for pure VBa-POSS was 142.6 J · g^{-1}, lower than that for pure VBa (423.2 J · g^{-1}); the exothermal peak of VBa-POSS (260 °C) was positioned at a higher temperature than that of pure VBa (207 °C) because of the dilution effect of the POSS units, which inhibited the thermal curing of VBa.[2,8] Figure 4 also displays DSC curves of pure VBa-POSS after

Macromolecular Journals
DOI: 10.1002/macp.201000362

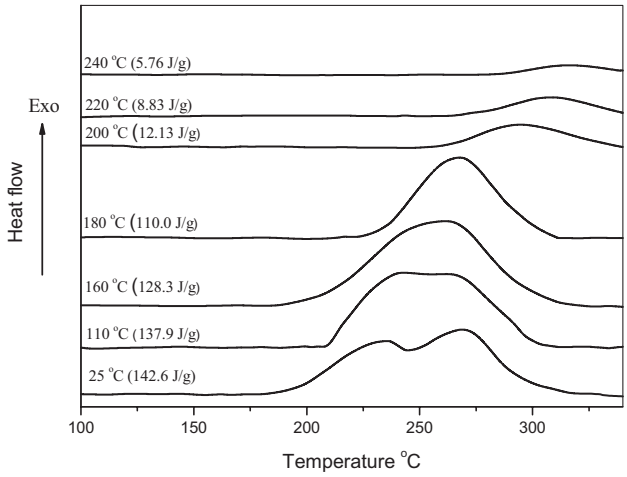

Figure 4. DSC curve of VBa-POSS recorded after each curing stage.

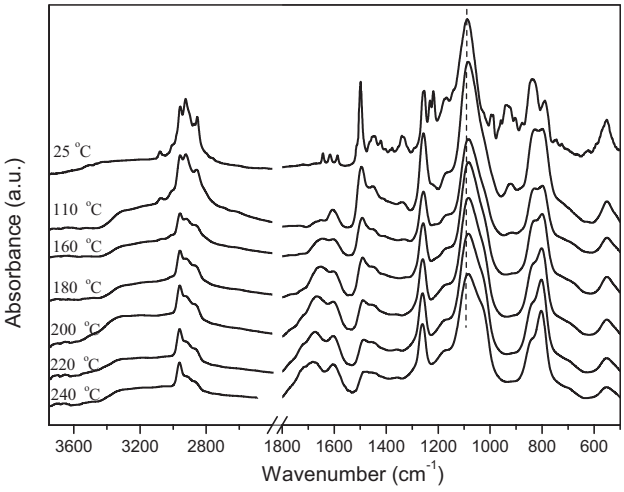

Figure 5. FTIR spectra of VBa-POSS recorded after each curing stage.

curing at various temperatures. The first exotherm, corresponding to the cross-linking of allyl groups, disappeared after curing at 200 °C. The intensity of the second exotherm decreased upon increasing the curing temperature, almost disappearing after curing at 240 °C.[10]

To ascertain which reactions were occurring during each exotherm in the DSC traces, we used FTIR spectroscopy to characterize the curing processes of the pure VBa-POSS systems at various temperatures. Figure 5 presents IR spectra recorded after each curing cycle of pure VBa-POSS. The characteristic absorption bands of the unsaturated allyl group (at 3 080 and 991 cm^{-1}) disappeared after curing at 180 °C (Figure 5a); in addition, a new band for the tetrasubstituted aromatic ring of the PVBa appeared at 1 480 cm^{-1}, with corresponding decreases in intensity of the bands representing the trisubstituted aromatic ring of VBa (1 498 and 943 cm^{-1}). The broad absorption bands at 2 500–3 500 cm^{-1} in Figure 5b–g represent three different kinds of hydrogen bonding interactions: $O^{-}\cdots H^{+}N$ intramolecular hydrogen bonding at ca. 2 750 cm^{-1}, OH···N intramolecular hydrogen bonding at ca. 3 200 cm^{-1}, and OH···O intermolecular hydrogen bonding at ca. 3 420 cm^{-1}; the identities of these signals have been discussed previously.[62] More importantly, the maximum peak position of the siloxane vibration band shifted from 1 089 cm^{-1} for the uncured VBa-POSS (Figure 5a) to 1 082 cm^{-1} after thermal curing (Figure 5b–g), suggesting that the siloxane groups of POSS interacted with the OH groups of the polybenzoxazine.[58]

Figure 6 presents FTIR spectra of pure VBa-POSS after curing at 180 °C for various lengths of time. The characteristic absorption bands of the unsaturated allyl group (3 080 and 991 cm^{-1}) and trisubstituted aromatic ring (1 498 and 943 cm^{-1}) of VBa-POSS disappeared during the early stages of curing (ca. 10–15 min). Here, we used 2D correlation spectroscopy to further characterize the interactions changes occurring to the pure VBa-POSS sample after various curing times. This approach, which treats the spectral fluctuations as a function of time, temperature, pressure, and composition, has been applied widely in polymer science[63–68] as a novel method for investigating the specific interactions between polymer chains. White and shadow areas in 2D IR correlation contour maps represent positive and negative cross-peaks, respectively.

Figure 7a presents the synchronous 2D correlation maps in the range 3 700–2 500 cm^{-1}. Our assignments of the absorption bands in this spectral range are discussed above (see Figure 5). Clear, positive cross-peaks existed between the all signals in this range, implying that all underwent changes in the same direction (i.e., they increased together)

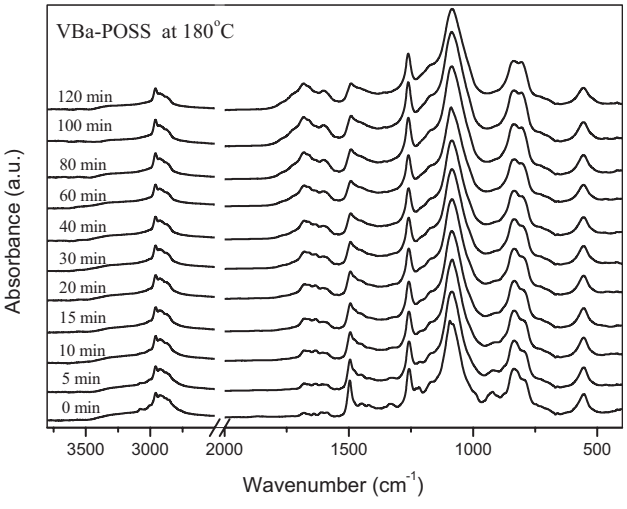

Figure 6. FTIR spectra of VBa-POSS after treatment at 180 °C for various curing times.

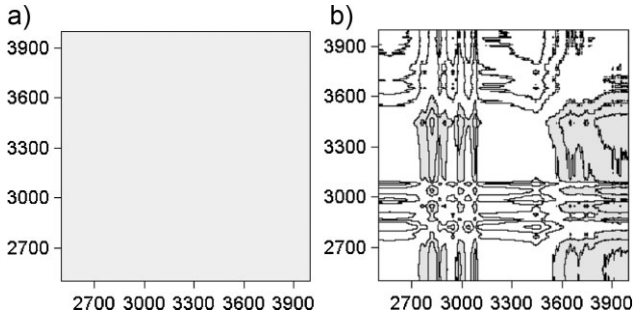

Figure 7. (a) Synchronous and (b) asynchronous 2D maps of the FTIR spectroscopic data for VBa-POSS treated for various curing times.

upon increasing the curing time, according to Noda's rule, because the degree of thermal curing increased upon increasing the curing time.[65] Figure 7b displays the asynchronous 2D correlation maps in the range 3 700–2 500 cm^{-1}. We observe no auto or cross-peaks within the ranges 2 700–2 500 cm^{-1} ($O^{-}\cdots H^{+}N$) or 3 400–3 200 cm^{-1} ($OH\cdots N$), implying that signals for intramolecular hydrogen bonding existed in these spectral ranges, consistent with our previous assignments. The cross-peaks between the signal at 3 400–3 200 cm^{-1} and those at 3 600–3 420 cm^{-1} in Figure 7b exhibit opposing intensity orders, indicating that these two bands result from different polymer chains, i.e., they represent intramolecular $OH\cdots N$ hydrogen bonding, intermolecular $OH\cdots O$ hydrogen bonding, and free OH groups. In addition, the positive peaks at 3 400–3 200 cm^{-1} in the asynchronous map of Figure 7b imply that the intensity of the signal at 3 200 cm^{-1} ($OH\cdots N$) altered before that at 3 420 cm^{-1} ($OH\cdots O$) upon increasing the curing time. Thus, the 2D map reveals that the sequence of changing intensity of these two bands was 3 200 > 3 420 cm^{-1}. The initial formation of intramolecular $OH\cdots N$ hydrogen bonds that later transformed into $OH\cdots O$ intermolecular hydrogen bonds upon increasing the curing time is consistent with results reported previously.[69]

Preparation of Polybenzoxazine/POSS Nanocomposites

Scheme 2 displays our approach toward the preparation of polybenzoxazine/POSS composites. Both the VBa monomer and VBa-POSS are soluble in THF and then this solution is allowed to dry in air prior to curing. Figure 8 displays the curing exotherms of neat VBa, neat VBa-POSS, and binary mixtures of the two at various weight ratios. Each curve features two exotherms – one corresponding to thermal curing of the allyl group, and the other to ring opening of the oxazine ring, as mentioned in our discussion of Figure 4 – indicating that the incorporation of VBa-POSS did not change the curing mechanism of neat VBa. Nevertheless, the maximum peak temperature shifted to higher temperature and the enthalpies of curing decreased upon increasing the VBa-POSS content in the polybenzoxazine/POSS nanocomposites. These results indicate that the presence of POSS moieties retarded the thermal curing of neat VBa because of a dilution effect of the randomly distributed POSS nanoparticles in the polybenzoxazine matrix, thereby decreasing the rate of curing relative to that of pure VBa.

Figure 9 presents the storage moduli (E') and loss tan δ curves of the PVBa and VBa-POSS hybrids incorporating various contents of VBa-POSS. The initial storage modulus of the unmodified PVBa was 3 280 MPa at 50 °C. The initial

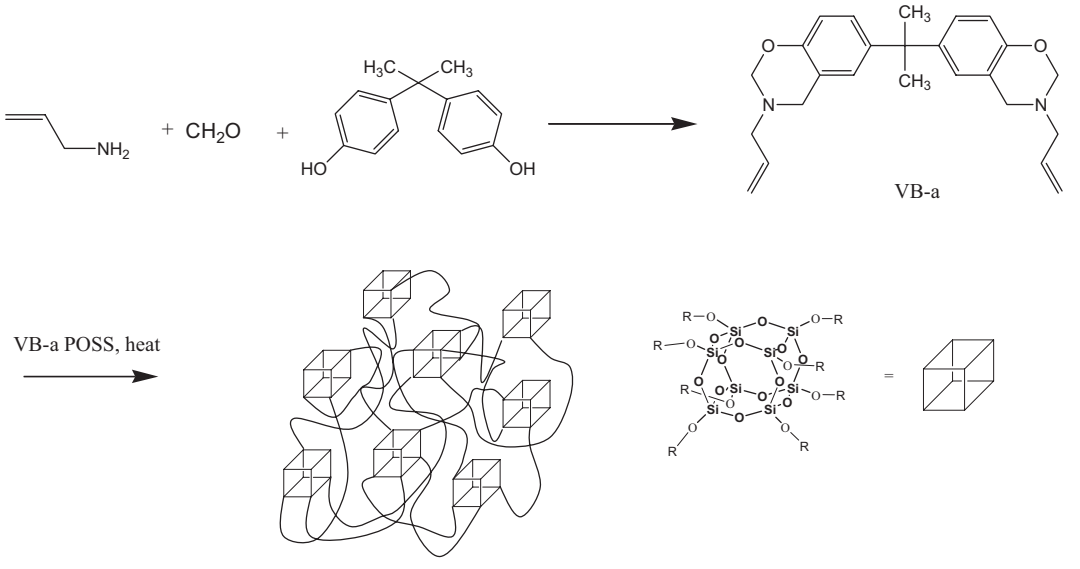

Scheme 2. Possible morphology for the VBa/VBa-POSS blends after thermal curing.

Macromol. Chem. Phys. **2010**, *211*, 2301–2311

Macromolecular Journals

DOI: 10.1002/macp.201000362

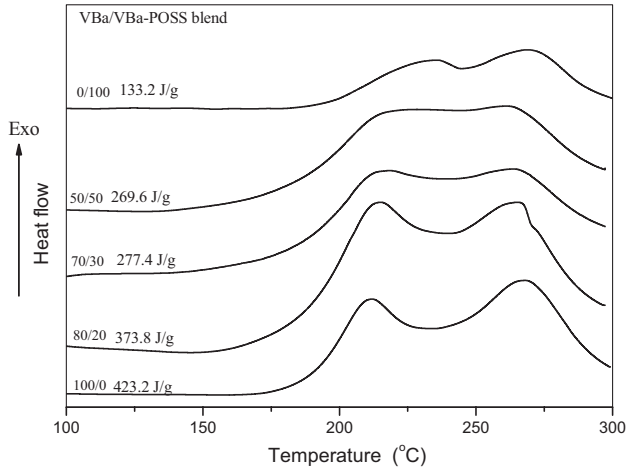

Figure 8. Curing behavior, determined through DSC analyses, of VBa/VBa-POSS mixtures containing various VBa-POSS contents.

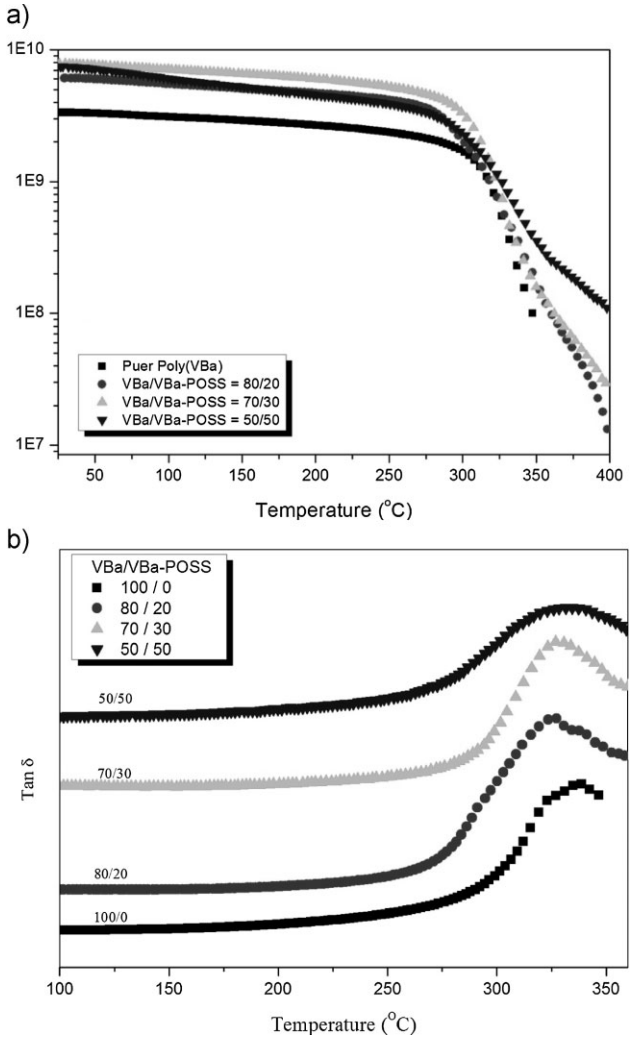

Figure 9. (a) Storage modulus and (b) tan δ of VBa/VBa-POSS blends containing various VBa-POSS contents, after curing.

values of E' of hybrids containing 20 and 30 wt.-% VBa-POSS were 5 970 and 7 640 MPa, respectively, at 50 °C; i.e., these values increased dramatically upon initially increasing the POSS content. The presence of the bulky and rigid POSS nanoparticles tended to stiffen the cross-linked polybenzoxazine network, thereby resulting in significant increases in the value of E'. Nonetheless, the nanocomposite incorporating a POSS content of 50 wt.-% exhibited a storage modulus less than that of the sample incorporating 30 wt.-% POSS, presumably because of two opposing effects of the POSS cages on the matrices. On one hand, the nanoreinforcement effect of POSS and the suppression of the molecular mobility on the polybenzoxazine matrix by bulky silsesquioxane groups will tend to increase the modulus of the material; on the other, the inclusion of POSS in the system will decrease the density of the nanocomposite. The increases in free volume of the nanocomposites are evidenced by the dispersion in their values of T_g. In these organic/inorganic hybrid materials, the cubic silsesquioxane core is rigid; its eight curable VBa groups are appended to the silsesquioxane core via Si—O linkages. In a network structure, the value of T_g relates directly to the cross-linking density.[70] The loss tan δ peak temperature in the DMA plot represents the glass transition temperature of the material. Figure 9b reveals a value of T_g for P(VBa) of 327 °C; those for hybrids containing 20, 30, and 50 wt.-% VBa-POSS are 326, 329, and 330 °C, respectively. Thus, the glass transition temperature did not change appreciably upon increasing the VBa-POSS content, due to the cross-link density of the system with varying POSS content hardly changed, similar to those affecting the storage moduli of these VBa-polybenzoxazine/POSS nanocomposites. In general, the value of T_g of a cross-linked network related its cross-linking density. As a result, the glass transition temperatures of these P(VBa)/POSS nanocomposites remained approximately constant. In previous studies reported by the Lee et al., for multifunctional benzoxazine (MBZ)-POSS contents of up to 10 wt.-% in Pa- or Ba-type hybrids, the aggregated MBZ-POSS units underwent macrophase separation, which reduced its overall effectiveness in hindering polymer movement. Thus, MBZ-POSS, which features an inorganic silsesquioxane core, appears to undergo serious aggregation during the polymerization process. In contrast, in this present study we could incorporate large amounts VBa-POSS – even 50 wt.-% – into VBa polybenzoxazine and still obtain transparent thin films. We used FTIR spectroscopy to confirm the presence of hydrogen bonding interactions in our polybenzoxazine/POSS nanocomposites containing various VBa-POSS contents as shown in Figure 10. The signals for the allyl groups (at 3 080 and 991 cm^{-1}) disappeared after thermal polymerization, indicating that similar polymerization reactions occurred as those observed to have occurred in Figure 5. Figure 10 displays expanded FTIR spectra (2 800–3 800 cm^{-1}) for various VBa/

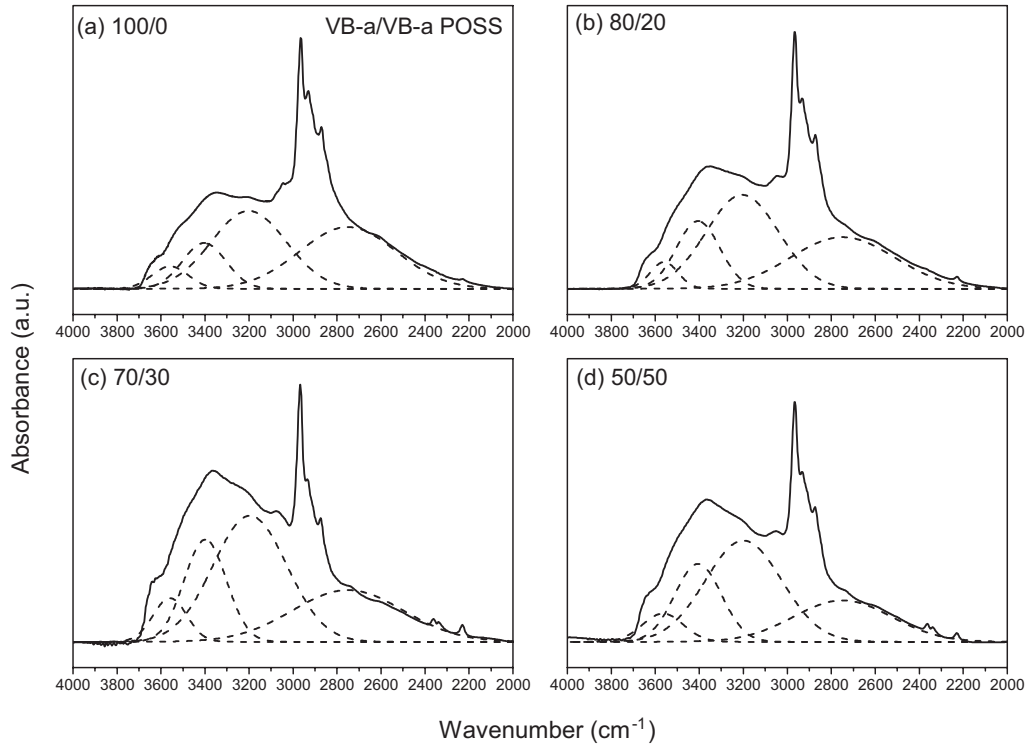

Figure 10. Curve fitting of FTIR spectroscopic data of VBa/VBa-POSS blends containing various VBa-POSS contents, after curing.

VBa-POSS copolymers after thermal polymerization at 180 °C for 4 h. Here, we assign four different kinds of environment for the OH groups: $O^{-}\cdots H^{+}N$ intramolecular hydrogen bonding at ca. 2 750 cm^{-1}, OH···N intramolecular hydrogen bonding at ca. 3 200 cm^{-1}, OH···O(ether) or OH···OSi intermolecular hydrogen bonding at ca. 3 420 cm^{-1}, and free OH groups. For better curve fitting, in this analysis we combine the effects of intermolecular the OH···O(ether) or OH···OSi hydrogen bonding interactions, which appear at similar wavenumber. Figure 10 presents the corresponding curve fitting data for the various VBa/VBa-POSS copolymers; Table 1 summarizes the results. Upon increasing the VBa-POSS content, the degree of OH···N intramolecular hydrogen bonding decreased, increased into OH···O(ether) or OH···OSi hydrogen bonds; thus, increasing the VBa-POSS content decreased the probability of intramolecular hydrogen bonding and enhanced the degree of intermolecular hydrogen bonding of the OH groups with the siloxane groups.

Figure 11 reveals the thermal stabilities of the polybenzoxazine/POSS nanocomposites under N_2; Table 2 summarizes the thermal properties. To compare the thermal stabilities, here we use the 20% weight loss

Table 1. Curve-fitting data for the signals of the OH groups in the FTIR spectra of the polybenzoxazine/POSS nanocomposites.

Sample	$O^{-}\cdots H^{+}N$		OH···N		OH···O or OH—O—Si		Free	
	ν	A_b	ν	A_b	ν	A_b	ν	A_b
	cm^{-1}	%	cm^{-1}	%	cm^{-1}	%	cm^{-1}	%
poly(VBa)	2 750	40.8	3 201	39.9	3 403	13.6	3 558	5.7
20 wt.-% VBa-POSS	2 749	33.8	3 204	42.9	3 405	18.5	3 559	4.8
30 wt.-% VBa-POSS	2 750	27.5	3 196	44.7	3 398	20.6	3 559	7.2
50 wt.-% VBa-POSS	2 749	24.4	3 199	46.6	3 405	21.9	3 562	6.1

Macromol. Chem. Phys. **2010**, *211*, 2301–2311

Macromolecular Journals

DOI: 10.1002/macp.201000362

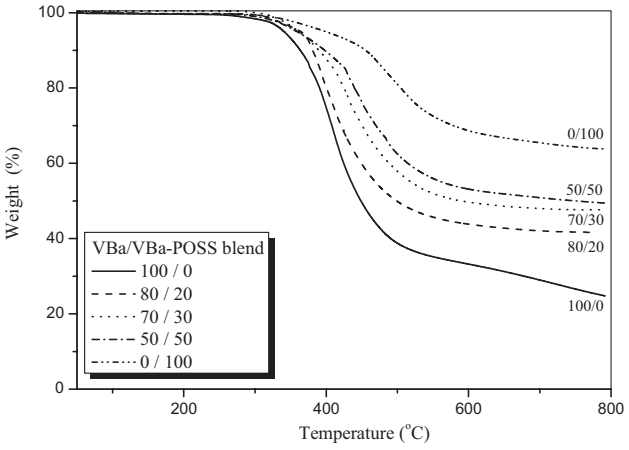

Figure 11. TGA analyses of VBa/VBa-POSS blends containing various VBa-POSS contents, after curing.

temperature as a standard. We observed a gradual increase in the decomposition temperature (T_d) of the polybenzoxazine/POSS nanocomposites upon increasing the VBa-POSS content, presumably because the effect of creating the nanocomposite. In a nanocomposite material, tethering of the components results in restricted thermal motion, thereby reducing the organic decomposition pathways accessible to the tether. The inorganic component (in this case, POSS) provides additional heat capacity, thereby stabilizing the materials against thermal decomposition. The char yield, another indicator of thermal stability, also increased upon the increasing the POSS content of these hybrid materials in the VBa monomers. Our results indicate that the thermal stability of polybenzoxazines is improved through the formation of network structures and because of the presence of the inorganic silsesquioxane. In these polymer/POSS nanocomposites, the POSS units might form a ceramic superficial layer during the early stages of combustion because of the low surface energy of the siloxane structure of POSS;[58] this ceramic layer would protect the underlying material by limiting heat transfer and hampering the diffusion of oxygen and the evacuation of combustible products – analogous to the behavior of layered silicates.

We used scanning and transmission electron microscopy (SEM and TEM, respectively) to examine the homogeneity of the POSS nanoparticle dispersion. The polybenzoxazine/POSS nanocomposite having a POSS content of 30 wt.-% exhibits (Figure 12a,d) a featureless morphology, with no discernible phase separation, suggesting that POSS nanoparticles were dispersed homogeneously throughout the matrix. Energy-dispersive X-ray (EDX) Si-mapping of all of the composites revealed that the particles were dispersed uniformly in the cross-sectional surfaces observed (Figure 12b,c); the gray points in the image denote POSS-enriched regions. When the concentration of POSS was 30 wt.-%, the Si-mapping micrograph revealed no aggregation; instead, it features many uniformly dispersed spherical particles.

Conclusion

We have synthesized a novel octafunctionalized VBa-POSS from octa-phenol POSS, formaldehyde, and allyl amine. VBa-POSS possesses cross-linking units that undergo polymerization with other VBa benzoxazine monomers, thereby allowing us to prepare new types of polybenzoxazine/POSS composites containing various POSS contents. TGA and DMA analyses revealed that the storage moduli and decomposition temperatures of these nanocomposites improved upon increasing the VBa-POSS content, due to hydrogen bonding interactions between siloxane groups of POSS and the OH groups of polybenzoxazine, as characterized through FTIR spectroscopic analysis.

Table 2. Thermal properties of poly(VB-a) and the poly(VB-a)/POSS nanocomposites.

Sample	DMA			TGA	
	G'	G''	tan δ	T_{20}	Char yield
	MPa[a)]	°C	°C	°C	%[b)]
poly(VBa)	3 304	311	327	390	24.7
20 wt.-% VBa-POSS	5 973	307	326	400	41.6
30 wt.-% VBa-POSS	7 642	306	329	425	47.6
50 wt.-% VBa-POSS	6 096	308	330	439	49.4
pure VBa-POSS	ND[c]	ND	ND	504	63.8

[a)]Measured at 50 °C; [b)]Measured at 800 °C; Pure VBa-POSS is not able to make a film.

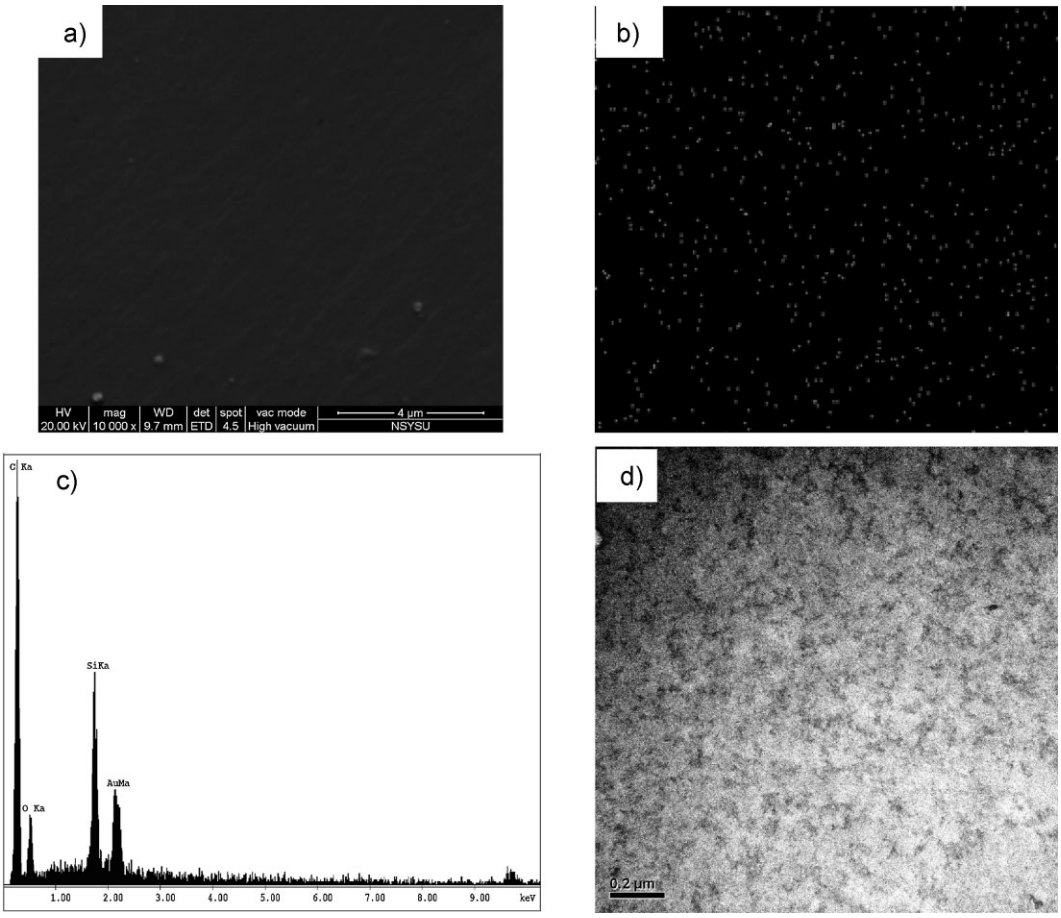

Figure 12. VBa/VBa-POSS = 70/30 after curing of (a) SEM image, (b) Si-mapping image, (c) EDX analysis, and (d) TEM image.

Acknowledgements: This study was supported financially by the *National Science Council, Taiwan, Republic of China*, under contracts no. NSC 97-2221-E-110-013-MY3 and NSC 97-2120-M-009-003.

Received: June 22, 2010; Revised: August 11, 2010; Published online: September 28, 2010; DOI: 10.1002/macp.201000362

Keywords: infrared spectroscopy; nanocomposites; thermal properties; thermosets

[1] X. Ning, H. Ishida, *J. Polym. Sci. Part A: Polym. Chem.* **1994**, *32*, 1121.
[2] T. Takeichi, T. Kawauchi, T. Agag, *Polym. J.* **2008**, *40*, 1121.
[3] C. P. R. Nair, *Prog. Polym. Sci.* **2004**, *29*, 401.
[4] N. N. Ghosh, B. Kiskan, Y. Yagci, *Prog. Polym. Sci.* **2007**, *32*, 1344.
[5] C. F. Wang, Y. C. Su, S. W. Kuo, C. F. Huang, Y. C. Shenn, F. C. Chang, *Angew. Chem. Int. Ed.* **2006**, *45*, 2248.
[6] C. F. Wang, Y. T. Wang, P. H. Tung, S. W. Kuo, C. H. Lin, Y. C. Sheen, F. C. Chang, *Langmuir* **2006**, *22*, 8289.
[7] C. F. Wang, S. F. Chiou, F. H. Ko, J. K. Chen, C. T. Chou, C. F. Huang, S. W. Kuo, F. C. Chang, *Langmuir* **2007**, *23*, 5868.
[8] A. Chernykh, T. Agag, H. Ishida, *Polymer* **2009**, *50*, 3153.
[9] T. Agag, T. Takeichi, *Macromolecules* **2001**, *34*, 7257.
[10] T. Agag, T. Takeichi, *Macromolecules* **2003**, *36*, 6010.
[11] T. Takeichi, K. Nakamura, T. Agag, *Des. Mono. Polym.* **2004**, *7*, 727.
[12] K. S. Kumar, C. P. Nair, T. S. Radhakrishnan, K. N. Ninan, *Eur. Polym. J.* **2007**, *43*, 2504.
[13] B. Kiskan, Y. Yagci, *Polymer* **2004**, *49*, 2455.
[14] B. Kiskan, B. Aydoan, Y. Yagci, *J. Polym. Sci., Part A: Polym. Chem.* **2009**, *47*, 804.
[15] A. Chernykh, T. Agag, H. Ishida, *Macromolecules* **2009**, *42*, 5121.
[16] S. W. Kuo, W. C. Liu, *J. Appl. Polym. Sci.* **2010**, *117*, 3121.
[17] S. Rimdusit, H. Ishida, *Polymer* **2000**, *41*, 7941.
[18] Y. C. Su, S. W. Kuo, H. Y. Xu, F. C. Chang, *Polymer* **2003**, *44*, 2187.
[19] J. M. Huang, S. W. Kuo, Y. J. Lee, F. C. Chang, *J. Polym. Sci. Polym. Phys.* **2007**, *45*, 644.
[20] T. Agag, T. Takeichi, *Polymer* **2000**, *41*, 7083.
[21] T. Takeichi, T. Agag, *Polymer* **2002**, *43*, 45.
[22] H. K. Fu, C. F. Huang, S. W. Kuo, H. C. Lin, D. R. Yei, F. C. Chang, *Macromol. Rapid Commun.* **2008**, *29*, 1216.
[23] G. Z. Li, L. C. Wang, H. L. Ni, C. U. Pittman, *J. Inorg. Organometal. Polym.* **2001**, *11*, 123.

DOI: 10.1002/macp.201000362

[24] S. H. Phillips, T. S. Haddad, S. J. Tomczak, *Curr. Opin. Solid State Mater. Sci.* **2004**, *8*, 21.
[25] M. Joshi, B. S. Butola, *J. Macromol. Sci. Polym. Rev.* **2004**, *C44*, 389.
[26] J. E. Mark, *Acc. Chem. Res.* **2004**, *37*, 946.
[27] K. Pielichowaski, J. Niuguna, B. Janowski, J. Pielichowski, *Adv. Polym. Sci.* **2006**, *201*, 225.
[28] P. D. Lickiss, F. Rataboul, *Adv. Organometal. Chem.* **2008**, *57*, 1.
[29] H. Xu, S. W. Kuo, J. S. Lee, F. C. Chang, *Macromolecules* **2002**, *35*, 8788.
[30] S. W. Kuo, H. F. Lee, W. J. Huang, K. U. Jeong, F. C. Chang, *Macromolecules* **2009**, *42*, 1619.
[31] S. W. Kuo, Y. C. Wu, C. H. Lu, F. C. Chang, *J. Polym. Sci. Polym. Phys.* **2009**, *47*, 811.
[32] C. F. Huang, S. W. Kuo, F. J. Lin, W. J. Huang, C. F. Wang, W. Y. Chen, F. C. Chang, *Macromolecules* **2006**, *39*, 300.
[33] C. H. Lu, F. C. Chang, S. W. Kuo, *Macromol. Chem. Phys.* **2010**, *211*, 1339.
[34] K. W. Huang, L. W. Tsai, S. W. Kuo, *Polymer* **2009**, *50*, 4876.
[35] A. Sellinger, R. M. Laine, *Macromolecules* **1996**, *29*, 2327.
[36] J. D. Lichtenhan, Y. A. Otonari, M. J. Carr, *Macromolecules* **1995**, *28*, 8435.
[37] L. Zheng, R. J. Farris, *J. Polym. Sci., Part A: Polym. Chem.* **2001**, *39*, 2920.
[38] A. Lee, J. D. Lichtenhan, *Macromolecules* **1998**, *31*, 4970.
[39] T. S. Haddad, J. D. Lichtenhan, *Macromolecules* **1996**, *29*, 7302.
[40] J. Zhang, R. Xu, D. Yu, *Eur. Polym. J.* **2007**, *43*, 743.
[41] Q. Chen, R. Xu, J. Zhang, D. Yu, *Macromol. Rapid Commun.* **2005**, *26*, 1878.
[42] C. Zhang, F. Babonneau, C. Bonhomme, R. M. Laine, C. L. Soles, H. A. Hristov, A. F. Yee, *J. Am. Chem. Soc.* **1998**, *120*, 8380.
[43] T. F. Baumann, T. V. Jones, T. Wilson, A. P. Saab, R. S. Maxwell, *J. Polym. Sci. Part A: Polym. Chem.* **2009**, *47*, 2589.
[44] R. S. Shih, C. H. Lu, S. W. Kuo, F. C. Chang, *J. Phys. Chem. C* **2010**, *114*, 12855.
[45] Y. Liu, S. Zheng, *J. Polym. Sci., Part A: Polym. Chem.* **2006**, *44*, 1168.
[46] Y. J. Lee, J. M. Huang, S. W. Kuo, J. K. Chen, F. C. Chang, *Polymer* **2004**, *46*, 2320.
[47] H. Y. Xu, S. W. Kuo, J. S. Lee, F. C. Chang, *Polymer* **2002**, *43*, 5117.
[48] Y. J. Lee, S. W. Kuo, Y. C. Su, J. K. Chen, C. W. Tu, F. C. Chang, *Polymer* **2004**, *45*, 6321.
[49] Y. J. Lee, J. M. Huang, S. W. Kuo, J. K. Chen, F. C. Chang, *Polymer* **2005**, *46*, 2320.
[50] Y. J. Lee, S. W. Kuo, C. F. Huang, F. C. Chang, *Polymer* **2006**, *47*, 4378.
[51] Q. Chen, R. W. Xu, J. Zhang, D. S. Yu, *Macromol. Rapid Commun.* **2005**, *26*, 1878.
[52] J. Zhang, R. W. Xu, D. S. Yu, *Eur. Polym. J.* **2007**, *43*, 743.
[53] Y. H. Liu, S. Zheng, *J. Polym. Sci., Part A: Polym. Chem.* **2006**, *44*, 1168.
[54] J. M. Huang, S. W. Kuo, H. J. Huang, Y. X. Wang, Y. T. Chen, *J. Appl. Polym. Sci.* **2009**, *111*, 628.
[55] Y. C. Wu, S. W. Kuo, *Polymer* **2010**, *51*, 3948.
[56] Y. J. Yen, S. W. Kuo, C. F. Huang, J. K. Chen, F. C. Chang, *J. Phys. Chem. B* **2008**, *112*, 10821.
[57] Y. C. Sheen, C. H. Lu, C. F. Huang, S. W. Kuo, F. C. Chang, *Polymer* **2008**, *49*, 4017.
[58] H. C. Lin, S. W. Kuo, C. F. Huang, F. C. Chang, *Macromol. Rapid Commun.* **2006**, *27*, 537.
[59] S. W. Kuo, H. C. Lin, W. J. Huang, C. F. Huang, F. C. Chang, *J. Polym. Sci., Part B: Polym. Phys.* **2006**, *44*, 673.
[60] L. J. Mathias, G. J. Tregre, *Polym. Compos.* **1997**, *18*, 509.
[61] L. J. Mathias, G. J. Tregre, *J. Polym. Sci., Part B: Polym. Phys.* **1998**, *36*, 2869.
[62] H. D. Kim, H. Ishida, *J. Phys. Chem. A* **2002**, *106*, 3271.
[63] I. Noda, Y. Ozaki, *Two-Dimensional Correlation Spectroscopy*, John Wiley & Sons, Hoboken 2004.
[64] S. W. Kuo, *Polymer* **2008**, *49*, 4420.
[65] I. Noda, *J. Am. Chem. Soc.* **1989**, *111*, 8116.
[66] S. W. Kuo, C. F. Huang, P. H. Tung, W. J. Huang, J. M. Huang, F. C. Chang, *Polymer* **2005**, *46*, 9348.
[67] S. W. Kuo, *Polymer* **2008**, *49*, 4420.
[68] I. H. Lin, S. W. Kuo, F. C. Chang, *Polymer* **2009**, *50*, 5276.
[69] S. W. Kuo, Y. C. Wu, C. F. Wang, K. U. Jeong, *J. Phys. Chem. C* **2009**, *113*, 20666.
[70] K. M. Kim, D. K. Keum, Y. Chujo, *Macromolecules* **2003**, *36*, 867.